Solar Energy 147 (2017) 37–51

Contents lists available at ScienceDirect

Solar Energy

journal homepage: www.elsevier.com/locate/solener

Experimental and numerical studies to assess the energy performance of naturally ventilated PV façade systems

Mehdi Shahrestani [a], Runming Yao [a,*], Emmanuel Essah [a], Li Shao [a], Armando C. Oliveira [b], Arif Hepbasli [c], Emrah Biyik [c], Teodosio del Caño [d], Elena Rico [d], Juan Luis Lechón [d]

[a] School of the Built Environment, University of Reading, Whiteknights, PO Box 219, Reading RG6 6AW, United Kingdom
[b] Centre for Renewable Energy Research, Faculty of Engineering, University of Porto, 4200-465 Porto, Portugal
[c] Department of Energy Systems Engineering, Faculty of Engineering, Yasar University, 35100 Bornova, Izmir, Turkey
[d] Onyx Solar, C/ Rio Cea 1-46, 05004 Ávila, Spain

ARTICLE INFO

Article history:
Received 6 April 2016
Received in revised form 4 February 2017
Accepted 20 February 2017

Keywords:
Building integrated PV façade (BIPV)
Ventilated PV façade
TRNSYS
PV system

ABSTRACT

This paper presents a holistic approach to assess the energy performance of a naturally ventilated PV façade system. A rigorous combined experimental and numerical approach is established. The real energy performance of the system has been evaluated through a long-term high resolution monitoring of a typical ventilated PV façade system. A numerical model based on TRaNsient SYstem Simulation (TRNSYS) package was developed to assess the thermal and energy performance of the system, which has been verified by a series of statistical analysis using the data collected from the experiment. The validated model was then used to assess the energy and thermal performance of a 7.4 kW_p prototype ventilated PV façade system in Izmir, Turkey. The results of this study demonstrated that ventilation in the air cavity of the PV façade system could significantly improve energy performance of the system even in a southeast facing façades. The quantitative analysis provides useful guidance to the system designers for the improvement of energy efficiency of the PV facade system.

1. Introduction

According to the international Kyoto protocol (1997), the UK government is committed to reduce greenhouse gas emissions by 30% and 80% below the 1990 level respectively by 2020 and 2050 (DECC, 2008). Utilising renewable technologies in buildings plays a significant role to achieve this commitment in the UK building sector. Based on the 2020 vision provided by the UK photovoltaic manufacturers association, utilising PV systems only on south-facing roofs and façades has the potential of generating 140 TWh/year electricity, which is almost 35% of electricity consumption in the UK (UKPV, 2009).

The first Building Integrated Photovoltaic (BIPV) system was installed in 1991 in Aachen, Germany (Benemann et al., 2001). At the beginning, the scale of installation of BIPV systems was around 5–10 kW_p. However, the installation of a 1 MW_p system at the Academy Mont-Cenis Herne was the beginning of an increasing demand for this system. Ventilated PV façade systems are one of the main arrangements of the BIPV systems that have been studied over the last two decades. One of the early studies in this field was conducted by Balocco (2002) in order to develop a simple model to assess the energy performance of the ventilated façade systems. Despite the huge success of the developed model in broadening the understanding of the energy performance of the ventilated PV façade systems; it was a steady-state model that assumed the velocity of the air within the air cavity based on the air temperature only. In addition, the outcomes of verification of the model with experiment were reported for just one representative day. In another study, Omer et al. (2003) assessed the actual performance of BIPV systems and compared the actual and predicted energy performance of two BIPV systems over a twelve-month period. The results of this study demonstrated a significant difference between the outcomes of PVSYST (a simulation tool) and experiment. This was mainly due to the effect of microclimate conditions on the energy performance of the system.

In an attempt to improve the accuracy of the numerical models in estimation of the energy performance of BIPV systems, Mei et al. (2003) developed a thermal model based on TRNSYS. This study addressed the dynamics thermal behaviour of the BIPV systems. However, it was only able to consider the effect of force ventilation within the air cavity of ventilated PV façade systems. In addition, the outcome of validation was only reported for a few representative days.

* Corresponding author.
E-mail address: r.yao@reading.ac.uk (R. Yao).

http://dx.doi.org/10.1016/j.solener.2017.02.034
0038-092X/

In another study, Infield et al. (2006) developed a simplified model to predict the thermal performance of the BIPV systems using steady-state analysis. Despite the simplicity of the model in analysing the thermal performance of BIPV systems, the force convective heat transfer within the air cavity was modelled empirically using the data collected from an experiment. This was one of the resultant limitations of the adopted approach in this simplified model, which made the model not suitable for naturally ventilated PV façade systems. In addition, the simplified model has not been validated with the experiment results.

Taking into account the effect of natural ventilation on the BIPV systems, Fossa et al. (2008) studied the thermal behaviours of the system in laboratory conditions. The results of experiment were compared with a numerical study, which revealed a very close correlation between the thermal behaviour of the system in both the experiment and the numerical model. However, in the experiment, a set of electrical resistances was used instead of PV modules, which could not be able to represent the thermal performance of PV modules especially under different irradiation levels. In another study, the natural convection in PV integrated double skin façade system was studied by Lau et al. (2011). However, the influence of natural ventilation was only reflected on the thermal behaviour of the system not the energy performance of the PV modules.

Han et al. (2013) evaluated the performance of ventilated double skin PV façades and compared the thermal performance of such a system with double skin façades. They developed a steady-state finite difference model and compared the simulation results with the outcome of a small-scale experiment. The results of this study demonstrated that ventilation in the PV façade reduced the possibility of potential overheating in hot weather conditions. However, the electrical performance of the PV façade has not been addressed and the validation of the model has been conducted for a steady state condition without reflecting on the thermal and energy performance of the system under dynamic and ever-changing weather conditions.

Gaillard et al. (2014) conducted an experimental study to assess the thermal and electrical performance of a naturally ventilated PV façade system. Airflow rate, irradiation and the system-generated power together with the amount of heat gained throughout the cavity of the PV façade system were provided in some typical days in each season. However, due to the pleated arrangement of the PV façade, the studied prototype ventilated PV façade could hardly represent the typical ventilated PV Façade systems. In addition, the holistic energy performance of the system including the annual electricity generation has not been addressed.

One of the most recent studies in this field has been carried out by Peng et al. (2016). They investigated the energy performance of the double skin PV façade system using both experiment and simulation. The simulation model was developed using EnergyPlus software and validated by experimental study between October and February. Despite, providing a holistic energy performance of the ventilated PV façade system, the developed model was validated only against the electricity generation and temperature of the PV modules respectively over 5 months and 1 week. In addition, a very significant influence of irradiation level on the efficiency of the PV modules (Skoplaki and Palyvos, 2009) has not been addressed.

From the literature review, it is evident that there have been a few studies that addressed the holistic energy performance of naturally ventilated PV façade systems to some extent. In addition, the developed numerical models to simulate the thermal and electrical performance of the ventilated PV façade systems were mainly focused on force ventilation regimes and were validated using experimental data collected over a limited period, which could not represent the varying operative conditions of the system. The aim of this research is to provide the holistic assessment of energy performance of a typical ventilated PV façade system through a rigorous numerical and experimental study. The outcomes of the experiment conducted over a period of ten months are used to verify the numerical model that is developed to assess the energy performance of the system. The verification of the model is conducted considering the energy performance of the system together with the most challenging parameters associated with ventilated PV façade systems including the PV surface temperature and airflow rate passing through the cavity of system.

2. Research design

This study is designed in three main parts. In the first part, an experiment is set-up to assess the performance of a typical ventilated PV façade system in real conditions. The details of experiments are provided in Section 3.

In the second stage, a numerical model is developed to predict the performance of the ventilated PV façade systems and the mode is verified using the experiment results. The numerical model is developed based on TRNSYS simulation package. The numerical model and its associated verification process are described in Sections 4 and 5 respectively. However, prior to the development of the model, a number of simulation packages including TRNSYS, ESP-r, PVSYST and EnergyPlus (Klein et al., 2009; EnergyPlus, 2011) were reviewed. In the open literature, several investigations in this field have been conducted through different simulation packages. Crawley et al. (2005 and 2008) conducted a comprehensive comparison study for the existing simulation packages. It shows that TRNSYS is one of the most appropriate tools for the study of the solar energy systems. In addition, in terms of software validation, TRNSYS is one of the listed simulation programs in the Building Energy Software Tools Directory of the US Department of Energy (DoE) and International Energy Agency (IEA) (Neymark and Judkoff, 2004). Moreover, several successful studies have been conducted using this tool (Kalogirou, 2001; Mei et al., 2003). Hence, the latest release of the TRNSYS simulation package (Version 17) is selected to assess the energy performance of the BIPV system in this study.

The last part of this study is designed to implement the verified model to assess the energy performance of a 7.4 kWp ventilated PV façade system in a Mediterranean weather conditions, in Izmir, Turkey, which is described in Section 6.

3. Experiment design

The experiment is set up on the Whiteknights campus of the University of Reading in the UK, 51.4°N, 0.94°W. It includes six Crystalline Silicon (c-Si) modules in two rows and three columns, installed on a South facing wood wall adjacent to the experiment shed. Location and geometry of the experiment is provided in Figs. 1 and 2.

The 150 mm air cavity between the PV modules and the back wood surface of the PV façade is naturally ventilated and air is passing through from three main openings of the façade; two openings at the top and bottom of the cavity and one gap between the first and second rows of the PV modules (Fig. 2). The thermal and physical properties together with electrical and optical properties of the PV modules are provided in Tables 1 and 2 respectively.

To assess the electrical efficiency of the PV modules at conditions other than 'Standard Test Conditions (STC)', two influential parameters are taken into account, which include the total irradiation level and PV module temperature.

The influence of PV module temperature on the electrical efficiency is considered using the following equation:

$$\eta_T = \eta_{stc} \times (1 - \beta \times (T - T_{stc})) \quad (1)$$

Location of Experiment: Whiteknights campus of the University of Reading, Reading, Berkshire, UK: 51.4407° N, 0.9448° W

Fig. 1. Location of the experiment site at the University of Reading.

where η_{stc} represents the efficiency of the PV module at standard test conditions and η_T stands for the efficiency of the modules under irradiation level equal to 1000 W m^{-2} and the PV module temperature equal to T (°C). According to the manufacturer information, the temperature coefficient (β) is equal to 0.0045 K^{-1}.

In addition, the influence of the total irradiation level on the electrical efficiency of the PV modules is considered using the following equation.

$$\eta_{irr-A} = \alpha \times \eta_{stc} \tag{2}$$

Where $\eta_{irr\text{-}A}$ stands for the electrical efficiency of the module under irradiation level equal to 'A' (W m^{-2}) and the PV module temperature equal to 25 °C. According to the manufacturer information, the irradiation coefficient (α) values are provided in Table 3.

As shown in Fig. 4, the PV modules are arranged in 3 columns each including two modules. Each pair of modules in each column is linked to a micro inverter with the maximum DC input power of 320 W, which matches with the total nominal peak power of the paired modules ($2 \times 155 = 310$ nominal peak power) provided in Table 2. It should be noted that the micro inverter has the capability of tracking the maximum power points through the Maximum Power Point Tracking (MPPT) system, which is included in the micro inverter (ABB, 2016). In this study, the electricity generation rates are recorded within the interphase of the inverter.

The experiment site comprises three principal physical elements as bellow:

1. Six Crystalline Silicon (CSi) PV modules,
2. Measuring instruments, and
3. Storage shed to host the data loggers and inverters.

These physical elements of the experiment are represented in a 3D drawing in Fig. 3. While, the actual experiment set up at the University of Reading is shown in Fig. 4.

The instruments used in this experiment (see Fig. 3) include:

- Twelve temperature sensors to measure the back surface temperature of the PV modules. Sensors are exposed to the air cavity (two sensors for each module)
- Six Thermo-Anemometers to measure the temperature and velocity of the air passing through the cavity (one sensor installed in the air cavity on the back of each module)
- A Pyranometer to measure total and diffuse irradiation levels on the vertical surface
- A radiometer to measure the total irradiation level on the horizontal surface
- A weather station to measure the outdoor temperature, relative humidity, wind speed and direction

Specification of these instruments is provided in Table 4.

4. Numerical simulation of the ventilated PV façade systems

Ventilation in PV integrated PV façades is driven by two principal forces: buoyancy or "the stack effect" and wind. In the former, the density of air is directly changed by air temperature. Increasing the air temperature decreases the density of the air and causing layers of air to be stacked. In ventilated PV façades, the air temperature inside the air cavity increases due to heat dissipation of the PV cell together with receiving solar radiation. The buoyancy of the warmer air provides a driving force to push the air up and set up an air circulation stream in the air cavity of the PV façade, which makes a naturally ventilated option for the façade system. The differential pressure driving force for natural ventilation across the air cavity opening of a typical ventilated PV façade system (Fig. 5) is provided in the following equations:

$$\Delta P_{L2} = P_{i2} - P_{o2} \tag{3}$$

$$P_{i2} = P_{i1} - g\int_{Z_{h1}}^{Z_{h2}} \rho_i(z)dz \tag{4}$$

$$P_{o2} = P_{ref} - g\int_{0}^{Z_{h2}} \rho_o(z)dz \tag{5}$$

$$P_{i1} = P_{ref} - g\int_{0}^{Z_{h1}} \rho_o(z)dz \tag{6}$$

where ΔP_{L2} is the differential pressure across the air opening on the top of the ventilated PV façade system. P_{ix} and P_{ox} respectively represent the pressure level in the cavity side and outside of the opening at level x. P_{ref} stands for the air pressure at the building reference level. Finally, ρ_i and ρ_o are the air density inside and outside the air cavity.

The wind pressure on a façade is the difference between the local pressure on the surface and the static pressure in the undisturbed wind on the same height. The wind pressure coefficient (Cp) is defined to relate this pressure difference to the dynamic pressure of the reference wind velocity at the building location and its reference height. Considering wind pressure coefficient in the Bernoulli's Equation, the wind pressure is calculated using the following equation:

$$\Delta P_w = \frac{1}{2} C_p \rho V_0^2 \tag{7}$$

where the wind pressure, ΔP_w (Pa), is the difference between wind pressure on the façade and the static pressure in the undisturbed wind on the same height and C_P is the wind pressure coefficient, ρ (kg/m^3) stands for the air density and V_0 (m/s) represents the reference wind velocity at the building location and its reference height.

In reality, location and pylon height of the meteorological station are usually different from the building location and building reference height. Considering the fact that the wind speed at the height of boundary layer is not location sensitive (Fig. 6), the velocity of wind at the top of the boundary in both building location and meteorological station are assumed the same ($V_{bm} = V_{b0}$). Therefore, the relation between the wind velocity at meteorological station and at building location is determined using the following equation (TRNFLOW, 2009).

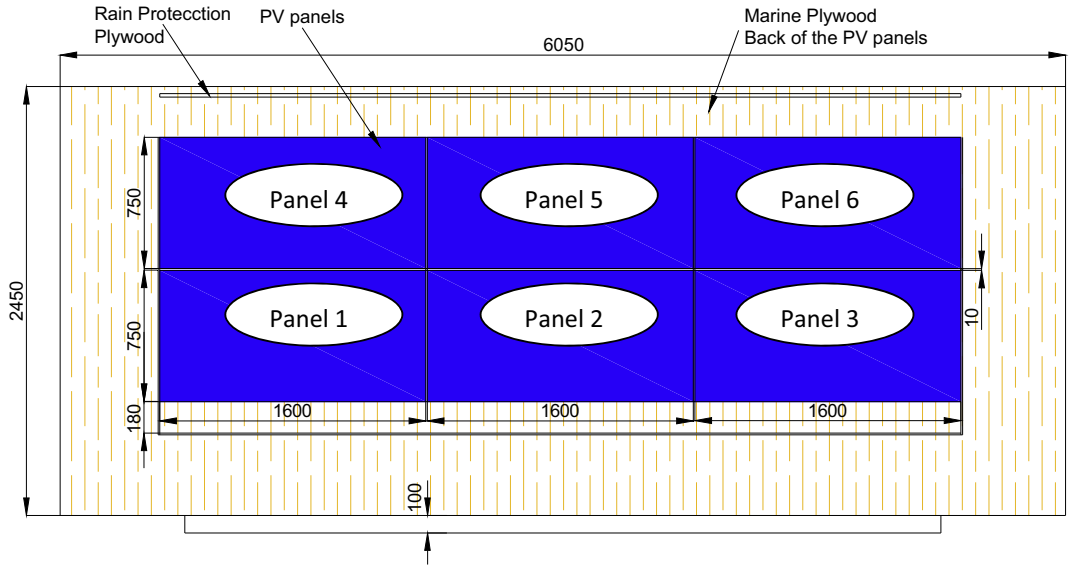

a) South View

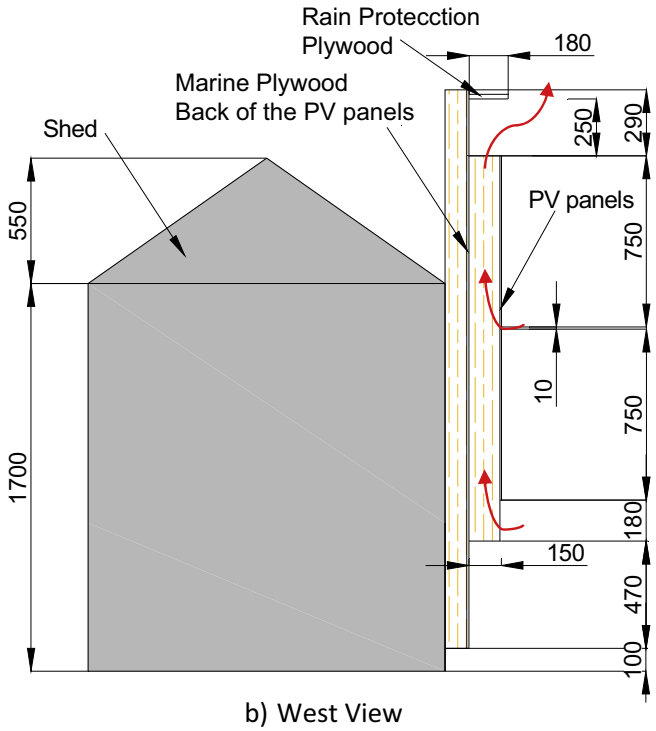

b) West View

Fig. 2. Geometry of the experiment in Reading (a) view from South (b) view from West (all dimensions in mm).

Table 1
Thermal and physical properties of different layers of the PV modules.

Layer/Property	Thickness (mm)	Thermal conductivity (W/m K)	Thermal capacity (J/kg K)
Glass-tempered	4	1	720
Monocrystalline silicon cell	<1	148	–
EVA layer	1.8	0.23	–
Glass- tempered	4	1	720

Note:
Dimensions of each module: 1600(L) × 750(W).
Percentage of area covered with photovoltaic cells in each module or active area of the module: 71.7%.
Weight density of the modules: 20 kg/m^2.

$$V_0 = V_m \left[\frac{h_b}{h_m}\right]^{\alpha_m} \times \left[\frac{h_0}{h_b}\right]^{\alpha_0} \quad (8)$$

where V_m, V_{bm} and V_{b0} (m/s) are respectively the wind velocity at meteorological station on pylon height, the wind velocity at meteorological station on boundary layer height and the wind velocity at building location on boundary layer height. h_m, h_b and h_0 respectively represent the pylon height at meteorological station, height of boundary layer and building reference height. Finally, α_m and α_0 stand for wind velocity profile exponent at meteorological station and building location respectively, which depend on the roughness of the terrain (Table 5). In addition, the height of the boundary

Table 2
Electrical and optical properties of PV modules (REELCOOP, 2015).

Electrical property	Value	Optical property	Value
Nominal peak power (P_{mpp})*	155 (Wp)	–Transparency degree (–)	30%
Open-circuit voltage (V_{oc})*	23 (V)	–Solar reflectivity for area without photovoltaic cells (–)**	6.8%
Short-circuit current (I_{sc})*	8.62 (A)	–Visible reflectivity for area without photovoltaic cells (–)***	7.9%
Voltage at nominal power (V_{mpp})*	18 (V)	–Solar transmissivity for area without photovoltaic cells (–)**	70.4%
Current at nominal power (I_{mpp})*	8.4 (A)	–Visible transmissivity for area without photovoltaic cells (–)***	86.8%
Power tolerance not to exceed (%)*	± 10%	–Solar reflectivity for area covered by photovoltaic cells (–)	14.8%
Maximum system voltage (V_{sys})	1000 (V)	–Visible reflectivity for area covered by photovoltaic cells (–)	7.6%
Operating temperature range	−40 to +85 (°C)	–Solar transmissivity for area covered by photovoltaic cells (–)	0%
Electrical efficiency of the module(–)*	15.5	–Visible transmissivity for area covered by photovoltaic cells (–)	0%
Electrical efficiency of the unit area of the module (–)*	12.9	Refractive index of the glass (–)	1.5

Notes:
* Measured properties at Standard Test Conditions (STC), 1000(W/m^2), a cell temperature of 25°C and air mass of 1.5, stabilised module state.
** Solar spectrum: 300–2500 nm.
*** Visible spectrum: 380–780 nm.

Table 3
Irradiation related coefficients for the electrical efficiency of the PV modules.

Irradiation level (W/m^2)	Irradiation coefficient α (–)
100	92%
200	97%
400	99%
700	102%
1000	100%

layer depends on the roughness of the terrain according to the following equations (TRNFLOW, 2009):

$$\begin{aligned} &if \quad \alpha_0 < 0.34, \quad h_b = 60\,\mathrm{m} \\ &if \quad \alpha_0 > 0.34, \quad h_b = 60\,\mathrm{m} + (\alpha - 0.34) \times (10800 \times (\alpha - 0.34) + 440) \end{aligned} \tag{9}$$

In Reading's experiment site the local weather station is set up at the experiment site and therefore, having local weather data, there is no need to transfer wind velocity from the meteorological

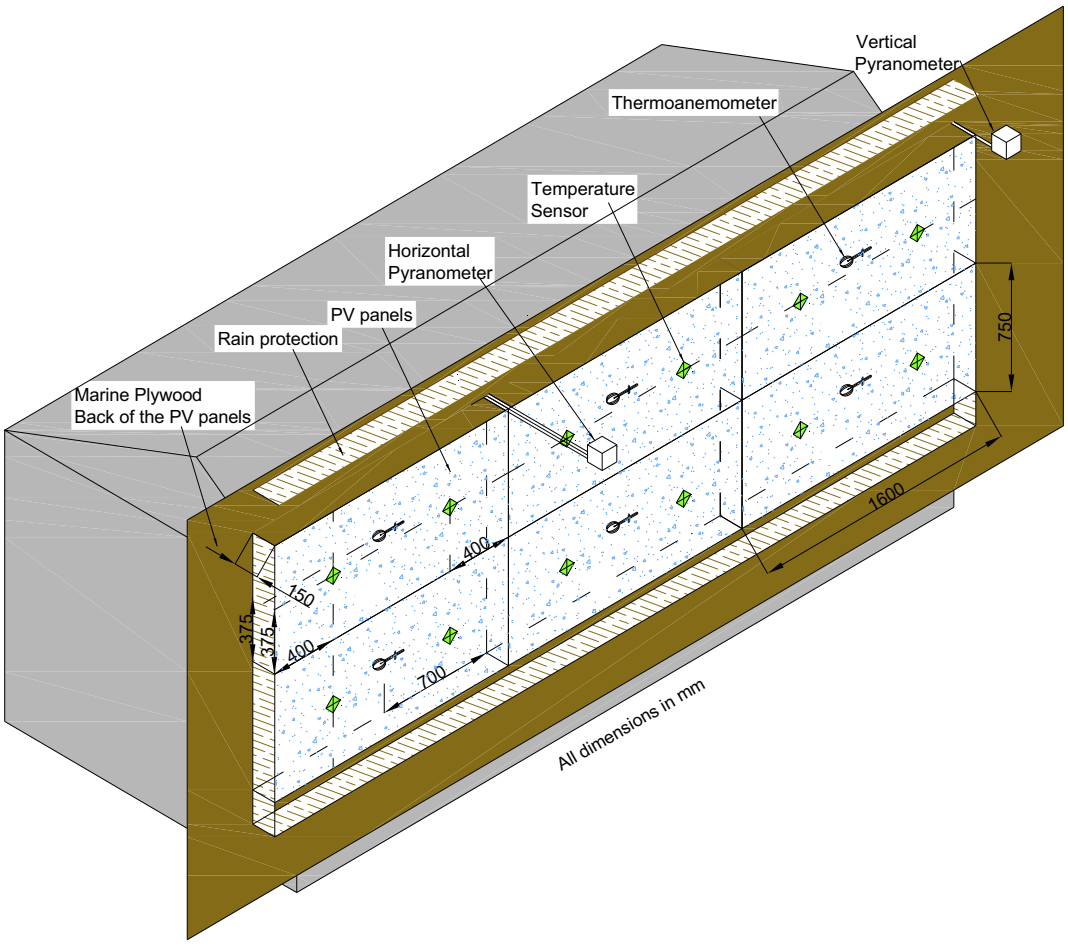

Fig. 3. The layout of physical elements of the PV monitoring set-up in Reading experiment (all dimensions in mm).

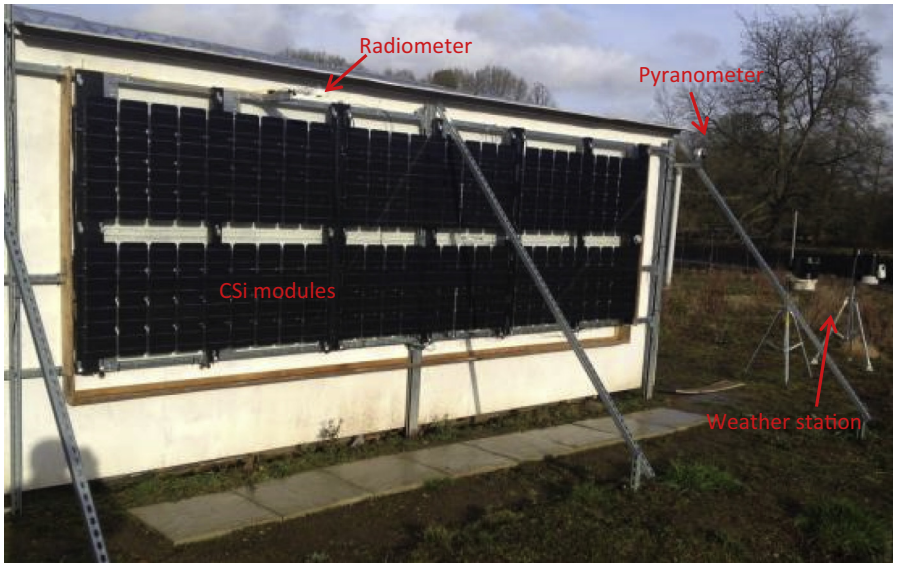

a) South view

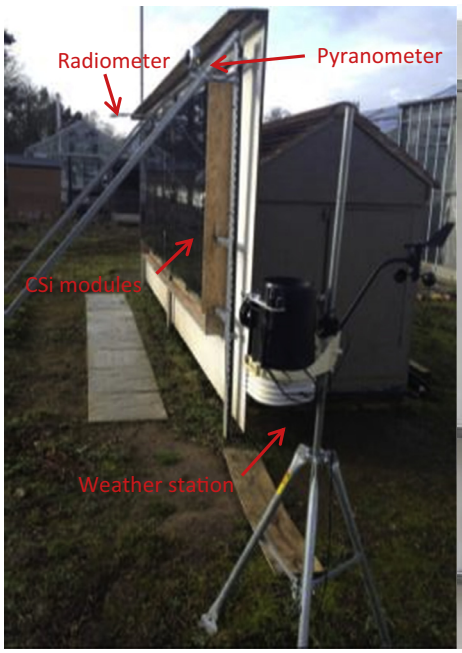

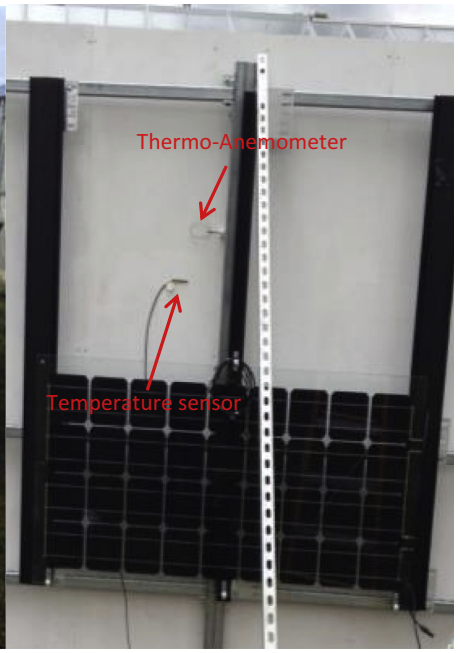

b) East view c) Instruments installed within the air cavity

Fig. 4. Prototype ventilated PV façade system at the University of Reading, (a) South view, (b) East view (c) instruments installed within the air cavity (back of each module).

station. Considering site location, roughness of the region is assumed in class 3 with a wind velocity profile exponent of 0.30 (Table 5). In addition, the wind pressure coefficients in different directions are defined according to a coefficient related to low rise buildings in a semi-shielded area (Orme et al., 1998; TRNFLOW, 2009). Considering these factors, the schematic diagram of the developed model for simulation of the PV ventilated façade system is provided in Fig. 7.

According to Fig. 7, the weather information including wind speed and direction are provided by a weather data file and are linked into a multi-zone energy model. For more accurate simulation, the air cavity on the back of each PV module is defined as a single zone with thermal interaction with each other as well as the PV modules. By increasing the temperature of the PV modules due to receiving solar radiation, part of this energy is being rejected into air cavity. This causes a rise in the air temperature of the cavity, which consequently reduces the density of the air that provides a driving force to push the air up due to the buoyancy of the warmer air. At the same time the multi-zone model of the system is linked to the TRNFLOW model (TRNFLOW, 2009) which is an airflow networking model developed based on COMIS (Feustel, 1999). The airflow model estimates the natural driving force of wind, which moves the air in the cavity considering the parameters including, the direction and speed of wind, geometry of the air cavity and orientation and size of the openings in the ventilated PV façade.

By integration of the airflow model and the multi-zone model in TRNSYS (TRNSYS, 2010), both the buoyancy and wind as the main driving forces for natural ventilation in the air cavity of the ventilated PV façade system are modelled simultaneously.

Table 4
Specification of instrumentation.

Description	Measurement range	Accuracy	Remarks
Temperature sensors (surface temperature measurement)	−55 °C to +125 °C	±0.5 °C	Digital Thermometer Model: DS18B20
Thermo-Anemometer (air temperature and flow rate measurement)	Velocity: 0–0.99 ms^{-1} 1–5 ms^{-1} Temperature: −20 to −0.01 °C 0–70 °C 70.01–80 °C	Velocity: ±0.04 ms^{-1} ±0.2 ms^{-1} Temperature: ±0.3 °C ±0.4 °C ±0.3 °C	Hotwire sensor Model: HD103T.0
Radiometer for measuring horizontal total irradiation(Total irradiation measurement)	300–2800 nm	<5% uncertainty (daily total) with 95% confidence level	Net Radiometer Model: CNR4
Pyranometer Vertical(Total and diffuse irradiation measurement)	400–2700 nm	±2% of incoming radiation over 0-90° Zenith angle	Sunshine Pyranometer Model: SPN1
Weather station	Temperature: −40 to 65 °C Wind speed: 0.5–80 ms^{-1} Wind direction: 0–360° Barometric pressure: 410–820 mm Hg	Temperature: ±0.5 °C Wind speed: 0.5% Wind direction: ±3° Barometric pressure: ±0.8 mm Hg	Model:Pro2

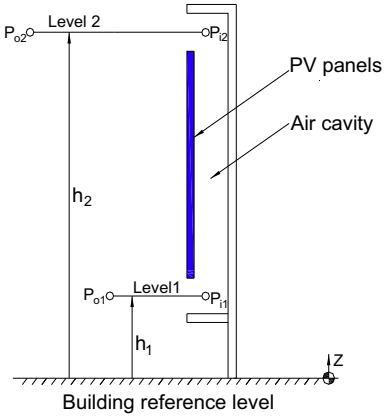

Fig. 5. Differential pressures within a ventilated façade system of the PV system.

Table 5
Roughness classes and their wind velocity profile exponents (Orme et al., 1998; TRNFLOW, 2009).

Class	Terrain description	Wind velocity profile exponent α_0
1	Sea, flat terrain without obstacles	0.10–0.15
2	Open terrain with isolated obstacles	0.15–0.25
3	Wood, small city, suburb	0.25–0.35
4	City centre	0.35–0.45

5. Verification of the numerical model and results of experiment

In order to check the credibility of the simulation, the results of the numerical analysis are compared with the outcomes of the experimental case study. In this analysis, the principal parameters associated with ventilated PV façade systems are considered to

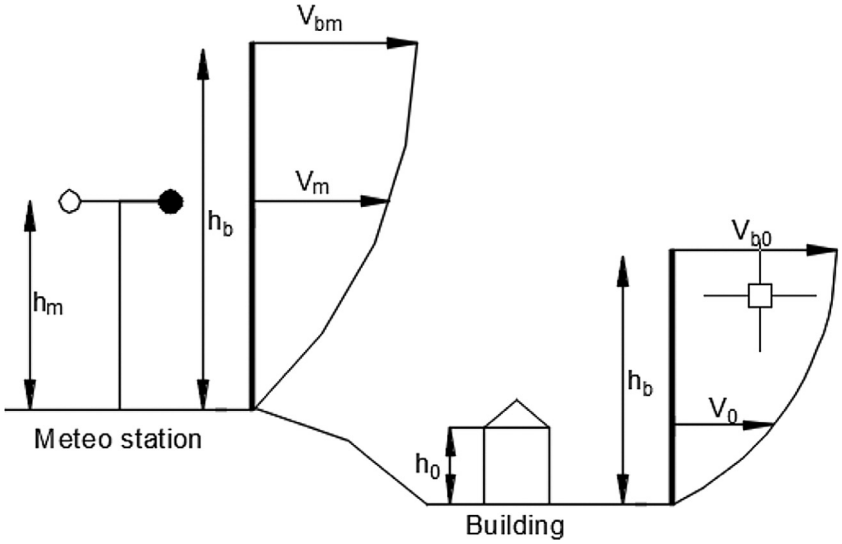

Fig. 6. Transfer of the wind velocity from the location of the meteorological station to the building location.

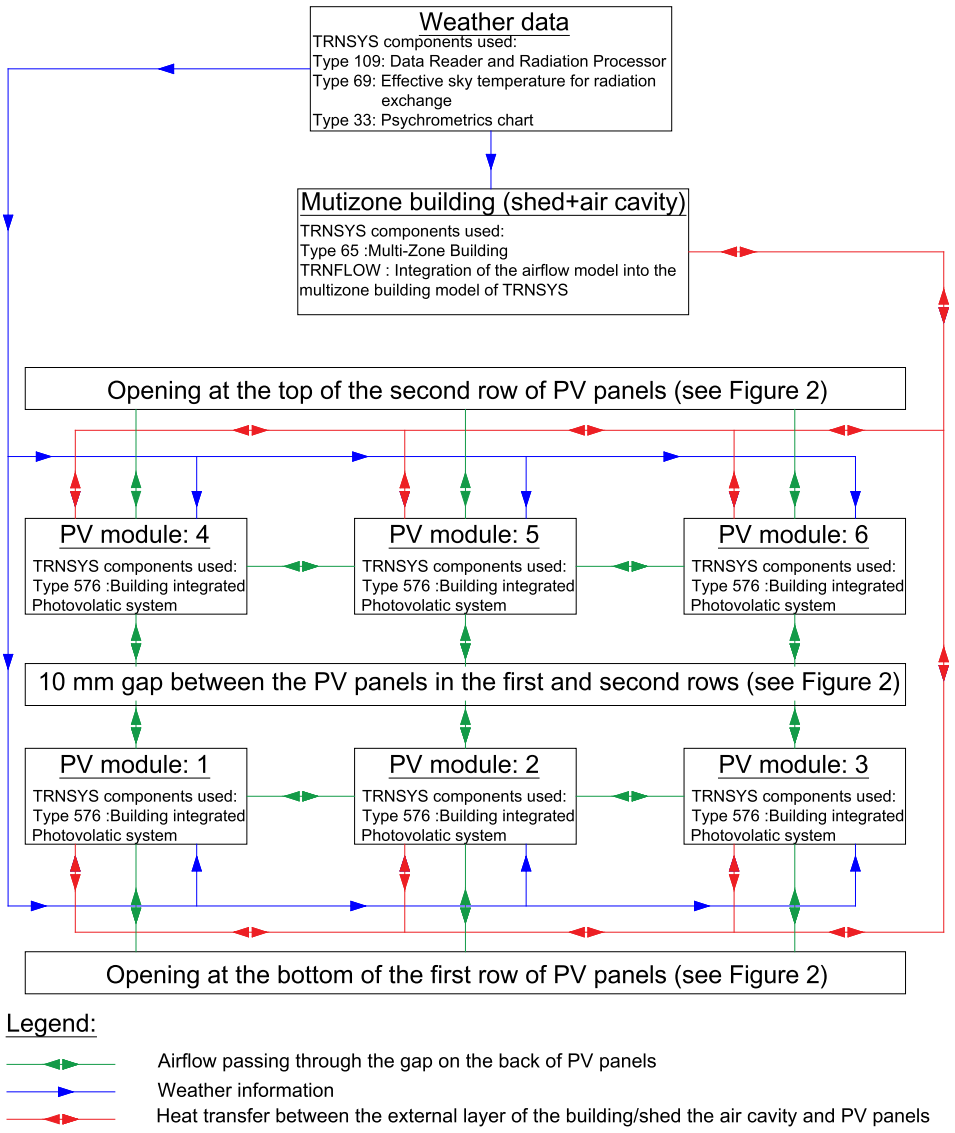

Fig. 7. TRNSYS schematic diagram for the simulation of the ventilated PV façade system. (See above-mentioned references for further information).

include generated electricity, surface temperature of the PV modules, and the flow rate of the air passing through the air cavity.

In terms of generated electricity, a comparison between the annual actual and predicted electrical energy generation values is demonstrated in Fig. 8. This figure shows a very close match between the outcomes of simulation and those recorded in the experiment with a maximum deviation of 11.2% in May and an average deviation of 5.8% between the annual predicted and actual electricity generation. In addition, Fig. 8 shows that both actual and predicted electricity generation values are following the trend of the recorded total irradiation level on the PV module surface.

From Fig. 8, the outcomes of the simulation underestimates the actual electricity generation of the system from April to September. This may be due to several factors including the accuracy of the irradiation coefficient (α) provided by manufacturer especially in higher irrational levels (Table 3) and the lower attitude angle of the sun in this period, which can cause more shading on the panels. This consequently increases the likelihood of experiencing more ununiformed shading and varies irradiation levels on the surface of PV modules and the pyranmometer.

In a higher resolution, the daily actual and predicted power generation of the ventilated façade system for a representative day in

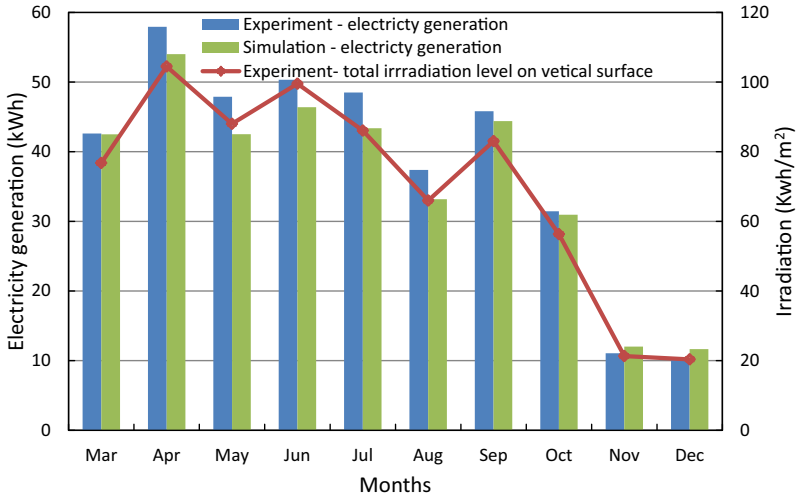

Fig. 8. Actual electricity generated compare to the simulation results together with the amount of irradiation on PV module surface (vertical).

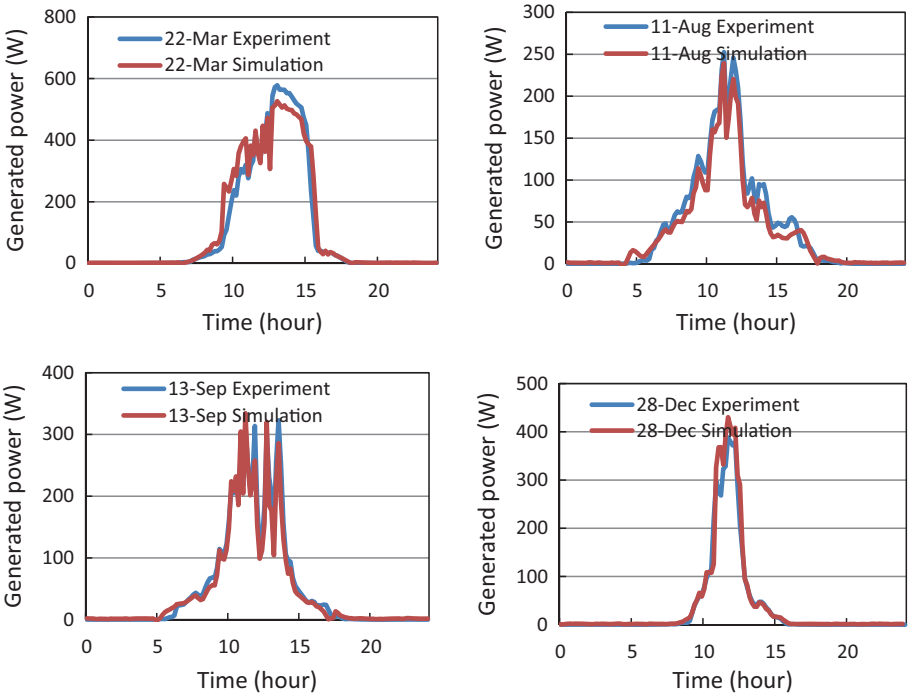

Fig. 9. Comparison of the actual power generation with numerical simulation results in four representative days in four seasons.

each season are illustrated in Fig. 9. This figure demonstrates a very good correlation between the simulation and experiment results associated with actual generated power and simulation results.

In order to check the robustness of the numerical predictive model, a statistical analysis is used to assess whether there is a statistical significant difference between the actual and predicted electrical energy generation values. The Wilcoxon rank sum as a non-parametric statistical hypothesis test is adopted mainly due to the fact that the electricity generation data is not normally distributed (Hollander and Wolfe, 1999; Gibbons and Chakraborti, 2014). In this test, the null hypothesis is that there is no statistical significant difference between the actual and predicted electrical energy generation values. To reject the null hypothesis, the statistical analysis should clearly demonstrate that 'P' value, which is the probability of observing a test statistic as or more extreme than the observed value, under the null hypothesis, is smaller than or equal to the significance level. Here, this level is defined as 0.05, which is a widely recognised value in statistical analyses.

The results of Wilcoxon rank sum test, given in Table 5, show that neither rank sum of two sets is less than or equal to the critical value for the Wilcoxon rank sum test, which is provided in Table 5. This critical value is related to the sample size, here, two sets (actual and predicted electrical energy generation values) each containing ten values (corresponding to each month, March to December). In addition, the P value is bigger than the 0.05, which demonstrates that based on the outcome this statistical analysis there is no evidence to reject the null hypothesis in this test. This implies that there is no statistical significant difference between the actual and predicted electricity generated values.

It should be noted that shadings associated with the metal structure used to set up the experiment and some instruments including the pyranometer used to measure the level of irradiation

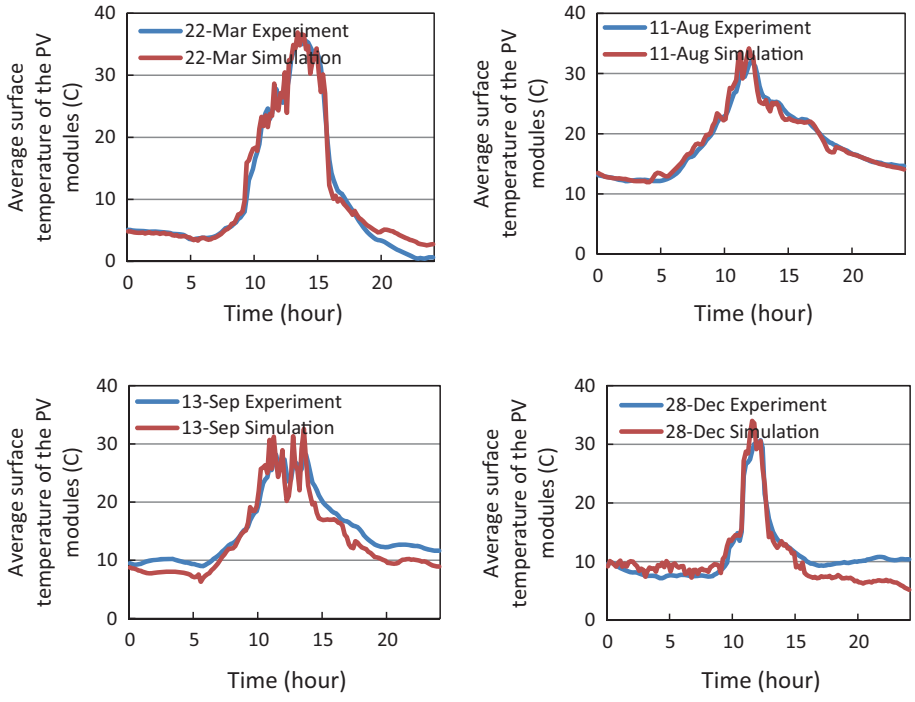

Fig. 10. Average surface temperature of PV modules, comparing simulation and experiment results in four representative days in four seasons.

on vertical surfaces (Fig. 4) are reflecting some level of uncertainty into the provided results.

Opposite to the electricity generation, monthly cumulative average temperature of the PV modules does not show a lot about the correlation between the results of experiment and numerical model. Therefore, these two sets of data are compared in a set of representative days for each season. Fig. 10 demonstrates the average surface temperature of the PV modules in experiment and numerical model. These results show that there is a very strong correlation between the average surface temperature of PV modules measured in the experimental study and those predicted by numerical simulation. In addition, in order to avoid any concerns over the extent in which those days can be representative of the whole period of study and also to provide a broad picture about the distribution of the data, statistical distributions of PV models surface temperature recorded in experimental study and predicted by the numerical simulation is provided in a box-and-whisker diagram (Fig. 11). This figure demonstrates a very reasonable and close interquartile ranges for the distribution of the experiment data and simulation in each season together with similar skewness of the data toward the high values in both datasets. The standard deviation and skewness of the both actual and predicted PV modules surface temperatures are provided in Table 6. Here, it should be noted that the normal distribution of the both actual and predicted PV surface temperature datasets were tested using Lilliefors test (Lilliefors, 1969). The outcomes of this test demonstrated that both datasets are not normally distributed. Therefore, the whiskers of box-and-whisker diagram (Fig. 11) are extended to the maximum and minimum of the range in the datasets.

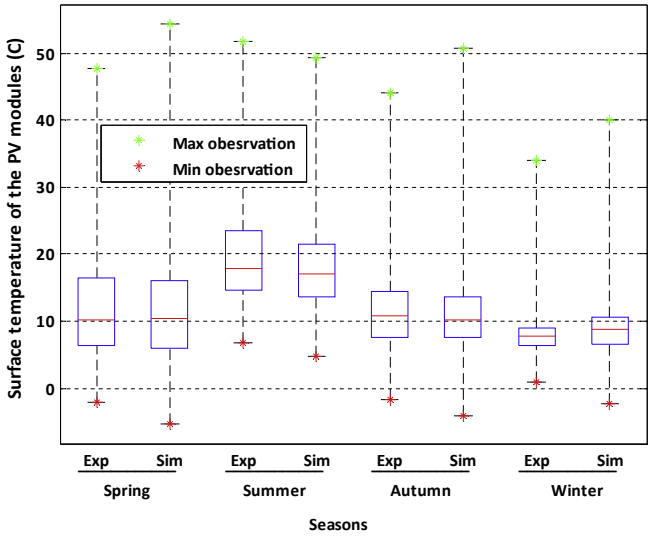

Fig. 11. Distribution of the surface temperature of the PV modules captured in the experiment and predicted in numerical analysis.

Here, it should be noted that the surface temperature of each module is approximately represented by the average of the measured values of two temperature sensors (Fig. 3) that measure the back surface temperature of each PV module.

In terms of airflow rate passing through the air cavity of the ventilated PV façade system, the outcomes of experiment and simulation are compared in Fig. 12. This figure is provided with a one-minute resolution of data for four representative days (one in each season) and revealed a very close correlation between these two datasets. However, it should be noted that due to the high level of accuracy and resolution of anemometer (Table 4) used to measure the air speed passing through the cavity accurately and fluctuating nature of the wind, these fluctuations are reflected on both datasets specially the experimental data.

In addition, in order to provide a broader picture about the distribution of data related to flow rate of air passing though the cavity of the ventilated PV façade system, the results of simulation and experiment are statistically illustrated in a seasonal box-and-whisker diagram (Fig. 13). A very close distribution of data in each quintile together with close interquartile ranges between experiment and simulation results demonstrates a good correlation

Table 6
Statistical verification of the predicted electricity generation of the system using Wilcoxon rank sum test.

Month	Electrical energy generated (kW h)		Rank	Electrical energy generated (kW h)	Rank	Electrical energy generated (kW h)
	Actual	Predicted				
Mar	**42.61**	42.50	1	**10.25**	11	**42.61**
Apr	**57.93**	54.02	2	**11.07**	12	43.37
May	**47.90**	42.52	3	11.66	13	44.39
Jun	**50.34**	46.40	4	12.03	14	**45.81**
Jul	**48.50**	43.37	5	30.96	15	46.40
Aug	**37.38**	33.17	6	**31.45**	16	**47.90**
Sep	**45.81**	44.39	7	33.17	17	**48.50**
Oct	**31.45**	30.96	8	**37.38**	18	**50.34**
Nov	**11.07**	12.03	9	42.50	19	54.02
Dec	**10.25**	11.66	10	42.52	20	**57.93**

Notes:
Critical value for Wilcoxon rank sum test (5% two-tail), corresponding to sample size: 78.
Sum of the rank of actual monthly electricity generation values: 113.
Sum of the rank of predicted monthly electricity generation values: 97.
Probability of observing a test statistic as or more extreme than the observed value, under the null hypothesis (p) is equal to 0.57. This value is more than 11 times bigger than the significance level of the statistic test that is equal to 0.05.

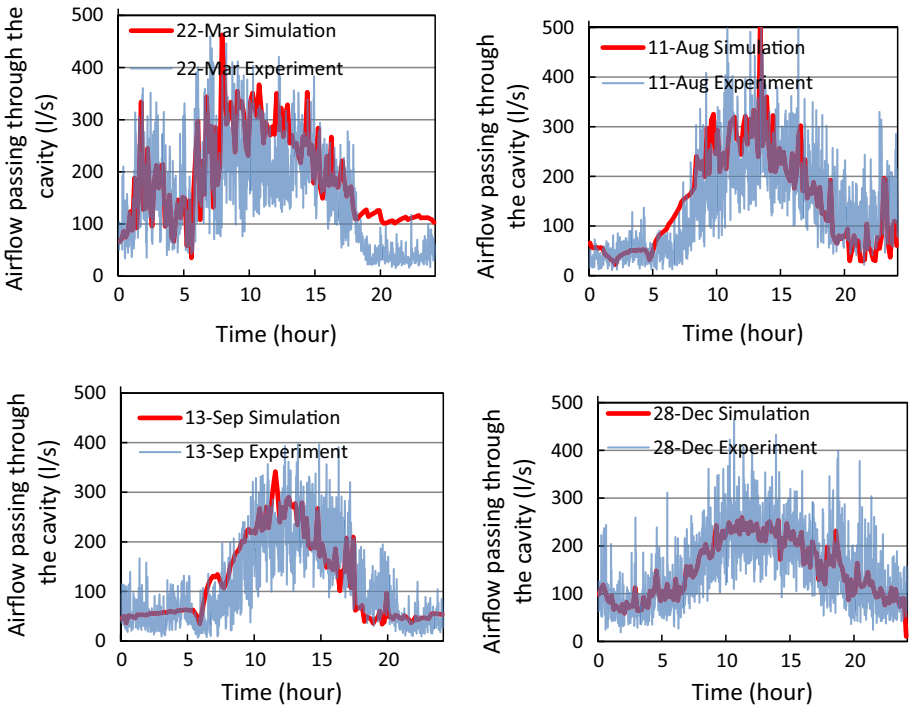

Fig. 12. Airflow rates of the air passing through the cavity of PV façade system, comparing simulation and experiment results in four representative days in four seasons.

between the experimental and simulation results. The seasonal box-and-whisker diagram provided in Fig. 13 demonstrates a tendency of the data to spread in high velocity reneges (third and fourth quartile) in both datasets in each season. This tendency is quantified in Table 7 by adopting the skewness of the datasets which are also very close between simulation and experimental data.

6. Energy performance of a case study ventilated PV façade system in Izmir

The verified numerical model is adopted to study the energy performance of a ventilated PV façade system in Yasar University, Izmir, Turkey. The candidate façade for installation of the PV façades is shown in Fig. 14. The building was constructed in 2013 and has an area of over 20,000 m^2. The candidate façade is a southeast facing façade of the building. The location of the building and the orientation of the façade are illustrated in Fig. 14.

The arrangement of the PV on the façade includes 48 Crystalline Silicon (c-Si) modules in 4 rows and 12 columns, which are shown in Fig. 15. Taking into account the peak power per PV module is 155 Wp (Table 2), this arrangement is designed to provide a 7.44 kW_p (48 PV modules) peak installed power.

The 150 mm air cavity between the PV modules and building exterior wall is naturally ventilated and air is passing through from the openings of the PV façade. One vertical linear opening (0.15 m × 1.6 m) is allocated at the top of all PV modules in rows 2 and 4. In addition, one linear horizontal opening (0.15 m × 1.6 m) is considered at the bottom of all PV modules in rows 1 and 3 respectively. Moreover, there is a 10 mm gap between

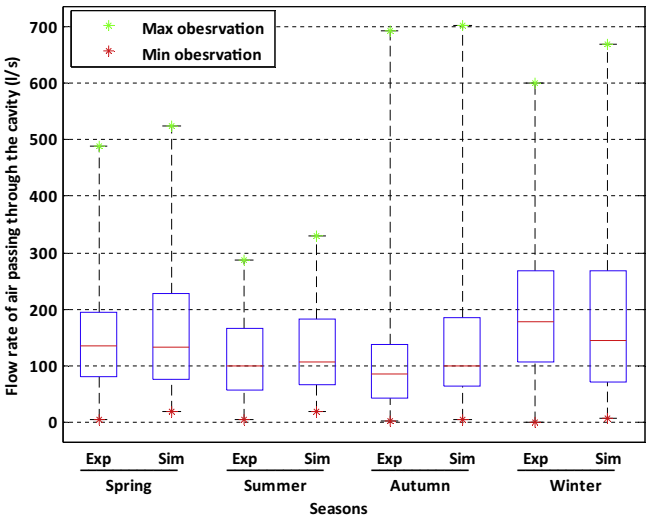

Fig. 13. Distribution of experimental and simulation results related to the airflow rate passing though the cavity of the ventilated PV façade system.

PV modules that contributes to the ventilation in the air cavity of the ventilated façade system.

Here it should be noted the model developed to assess the energy performance of ventilated PV façade systems in this study is a physical model. In the physical models, including the model developed in this study, the boundary conditions and weather data are defined based on local microclimates and weather conditions and the outcomes are driven by the local conditions defined rather than the condition in which the model is verified (Mellit et al., 2014; Dolara et al., 2015).

Summary of the simulation results is provided in Table 8. In this façade arrangement (Fig. 15), the surface temperature of PV modules can reach up to 51.2 °C. Considering the annual predicted electricity generation and the annual cumulative irradiation level, the total annual electrical efficiency of the BIPV system per square meter of modules and per square meter of active area are 9.2% and 12.6%, respectively. In addition, shading from surrounding buildings/obstructions reduces the amount of irradiation levels on PV modules by 23.5% to 39.7% for the modules installed in rows 1–2 and 3–4 respectively. Investigating the influence of natural ventilation on the energy performance of the system revealed that

Table 7
Standard deviation and skewness of the surface temperature of the PV modules recorded in the experiment and predicted in numerical analysis.

Season	Standard deviation		Skewness	
	Experiment	Simulation	Experiment	Simulation
Spring	8.9	8.6	1.2	1.2
Summer	7.9	7.1	1.3	1.2
Autumn	7.2	8.2	1.3	1.9
Winter	3.3	3.9	1.2	2.0

Fig. 14. Candidate building to install ventilation PV façade system in Yasar University, Izmir, Turkey (REELCOOP, 2015).

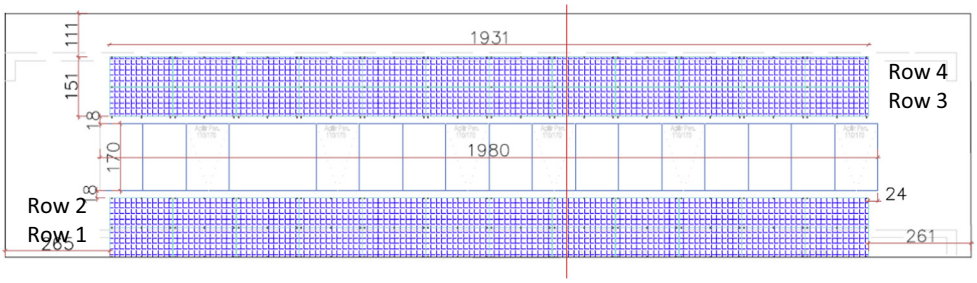

Fig. 15. Studied arrangement of PV façade at Yasar University, Izmir, Turkey, all dimensions in mm (REELCOOP, 2015).

Table 8
Standard deviation and skewness of the experimental and simulation results related to the airflow rate passing though the cavity of the ventilated PV façade system.

Season	Standard deviation		Skewness	
	Experiment	Simulation	Experiment	Simulation
Spring	85.0	96.6	0.6	0.8
Summer	67.7	70.5	0.5	0.6
Autumn	79.4	89.1	1.9	1.6
Winter	119.0	132.6	0.5	0.9

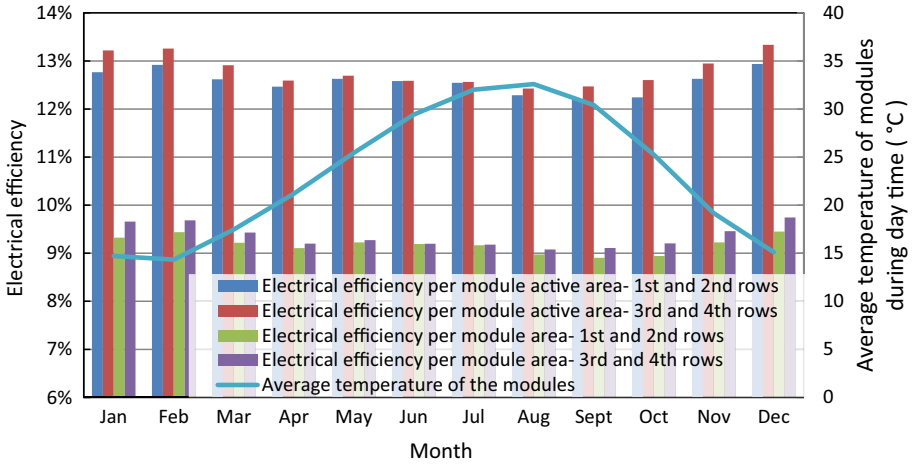

Fig. 16. Electrical efficiency per module area and the average temperature of the c-Si PV modules on southeast facing façade of the building at Yasar University campus, Izmir, Turkey.

Table 9
Performance of c-Si PV modules under the new arrangement of BIPV system on the southeast facing façade of building Y at Yasar University campus, Izmir, Turkey.

Characteristics		Modules			
		Row 1	Row 2	Row 3	Row 4
Annual average surface temperature of the PV modules in each row (°C)	Maximum	51.16	51.27	51.13	51.15
	Minimum	−4.96	−5.04	−4.44	−4.35
	Average	18.08	18.36	18.38	18.57
Average of annual irradiation on the surface of the PV modules in each row (kW h/m^2), Notes 1 and 2		689	726	852	875
Annual shading factor in each row, Notes 1 and 3		39.7%	36.5%	25.5%	23.5%
Annual electricity generated (kW h), Notes 1 and 2		1863		2319	
Total annual electrical efficiency of the ventilated PV façade system per square meter of modules, Notes 1, 2 and 3		= (1863 + 2319)/((689 + 726 + 852 + 875)/4 * 57.6) = 9.2%			
Total annual electrical efficiency of the ventilated PV façade system per square meter of active area of the module, Notes 1, 2 and 3		= (1863 + 2319)/((689 + 726 + 852 + 875)/4 * 42.08) = 12.6%			
Total annual electricity generated with assuming no ventilation in air cavity (kW h)		4092			
Percentage of increase in the annual electricity generation by providing ventilation in the air cavity of PV façade		2.2%			
Total annual electricity generated with assuming no shading from surrounding buildings and/or obstructions (kW h)		5409			
Total annual electricity generated with assuming no shading from surrounding buildings and/or obstructions and no ventilation in the cavity (kW h)		5203			
Percentage of increase in the annual electricity generation by providing ventilation in the air cavity of PV façade without shading		4%			
Total annual electricity generated with/without shading from surrounding buildings and/or obstructions and 230–460 l/s ventilation on the back of each PV module in the air cavity (kW h)		With shading: 4233–4264 Without shading: 5446–5501			
Percentage of increase in the annual electricity generation by providing 230–460 l/s ventilation back of each PV module in the cavity (with/without shading)		Withshading: 3.4–4.2% Without shading: 4.7–5.7%			

Note:
1. Weather conditions at site are considered based on the Meteonorm database for Izmir. Shading caused by surrounding buildings is taken into account.
2. The losses associated with the connections and Balance of System (BOS) are not included.
3. Shading factor is the amount of irradiation, which does not reach the PV modules due to shading by surrounding buildings/obstructions divided by the maximum possible irradiation (without shading) on the surface of the modules. The annual irradiation level on the vertical surface without shading is equal to 1144 (kW h/m^2).

natural ventilation can contribute to 2.2% increase in the annual energy generation of the system (Table 8). In case that the shading from surrounding buildings and obstructions are excluded, the natural ventilation in the air cavity, contributes to 4% increase in the annual energy generation of the PV façade system. In addition, simulation results provided in Table 8 demonstrate that fixed

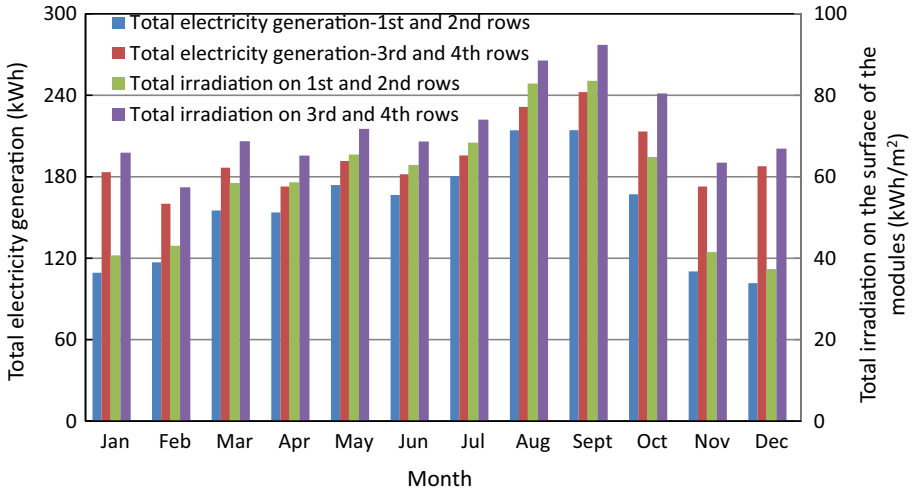

Fig. 17. Total electricity generation and total irradiation level on c-Si PV modules on southeast facing façade of the building at Yasar University campus, Izmir, Turkey.

ventilation rates equal to 230 and 460 l/s on the back of each PV module increase the annual electricity generation of the system up to 4.7–5.7% respectively. The monthly electrical efficiency profile of the system considering the active area of the modules (with shading) is demonstrated in Fig. 16. It should be note that the electrical efficiency addressed in this paper is defined as the amount of electricity generated (kW h) divided by the irradiation (kW h) on the surface of the PV modules at the same period.Table 9

In addition, Fig. 17 demonstrates the total electricity generation and irradiation levels considering shading from surrounding buildings. In this figure the total generation and irradiation levels during August and September are the highest. However, in these two months the electrical efficiency of the modules is up to 0.7% lower than its maximum value in December (Fig. 16). This is mainly due to the fact that the temperature of the PV models has significant influence on the electrical efficiency of the system; which is demonstrated in Fig. 16. This figure reveals a meaningful opposite trend between surface temperature and the electrical efficiency of the modules, which addressed in the open literature (Skoplaki and Palyvos, 2009) and reflected on the simulation results. For example, in August we both have the highest average modules temperature during daytime and the lowest electrical efficiency for the modules in the top two rows (Fig. 16).

In addition, the monthly performance ratio of the ventilated PV façade system is assessed. Performance ratio (PR) is stated as percentage and describes the relationship between the real and the theoretical possible electrical energy output of the system. It shows the proportion of the electrical energy that is actually available for export to the grid after deduction of energy losses. The closer the PR value for a PV system approaches 100%, the more efficient the respective PV system is operating. The performance ratio is determined based on the following Equations:

$$\text{Performance Ratio(PR)} = \frac{E_A}{E_T} \times 100 \tag{10}$$

$$E_T = E_A \times \eta_{stc} \times A \tag{11}$$

$$\eta_{stc} = \frac{\text{Nominal peak power of each module}}{\text{Area of each module}} \tag{12}$$

where E_A (kW h) represents the actual electrical energy generated by the system; E_T (kW h) is the theoretical electrical energy output of the system; I_A (kW h/m^2) is the actual irradiation level per square meter; A (m^2) is the total area of the PV modules in the ventilated PV façade system and η_{stc} (–) stands for the nominal efficiency of the PV modules at standard test conditions (Table 2). Fig. 18

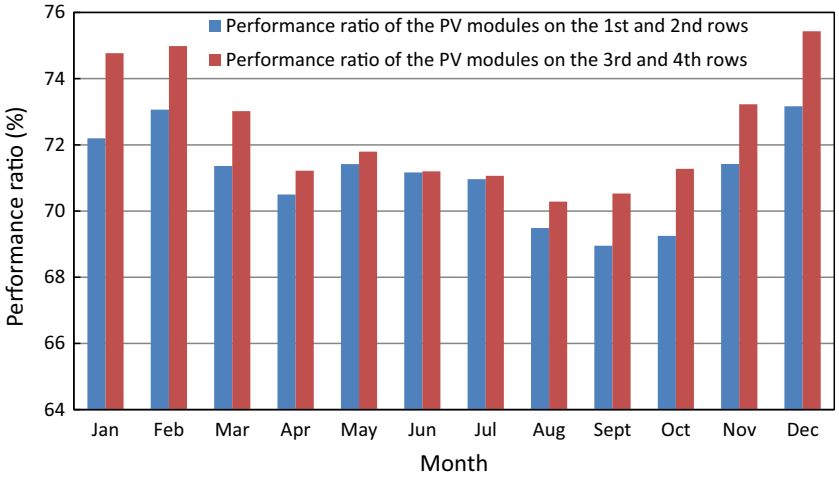

Fig. 18. Performance ratio of the c-Si PV modules on southeast facing façade of the building at Yasar University campus, Izmir, Turkey.

demonstrates that the performance ratio of the PV modules in the first and second two rows are in the range of 69–73% and 70–75% with an average of 71% and 72% respectively.

7. Conclusions

In this research, a rigorous combined experimental and numerical approach were developed to assess the energy and thermal performance of the naturally ventilated PV façade systems. The energy and thermal characteristics of a prototype ventilated PV façade system were measured with a high resolution of one minute interval in four seasons. Apart from providing a very clear energy performance of the system in outdoor real conditions as a reference, the outcomes of the experiment formed a reliable database, which were used to verify a numerical model developed to predict the energy and thermal performance of the ventilation PV façade system. Verification of the model was conducted against the actual data collected in four seasons, which demonstrate the robustness of the numerical approach not only in a very limited period but almost a year. The verified model was then used to predict the holistic energy and thermal performance of a 7.4 kWp ventilated PV façade system in Izmir, Turkey. The outcomes of this study revealed that, ventilation of the PV façade system can contribute to more than 2% increase in the annual electricity generation of the system even in southeast facing façades under about 31% shading in Mediterranean weather conditions. In addition, considering the studied case without shading in the same orientation shows that the ventilation improves the efficiency of PV façade system up to 4%. Also, fixed ventilation rates equal to 230 and 460 l/s on the back of each PV module increase the annual electricity generation of the system up to 4.7 to 5.7% respectively. All these demonstrate that considering ventilation for the PV façade system can significantly improve the total energy performance of the system even in southeast facing façades. The established combined experimental and numerical approach is rigorous which could be referenced by other similar studies. The effectiveness of ventilation is significant on energy performance of a PV integrated façade. The quantitative analysis provides useful guidance to the designers for the improvement of efficiency of the PV facade system.

Acknowledgment

This study is part of the Research Cooperation in Renewable Energy Technologies for Electricity Generation (REELCOOP) project co-ordinated by Professor Armando Oliveira from the University of Porto and led by Workpackage leader Professor Runming Yao from the University of Reading. The authors would like to acknowledge the financial support of the EU commission on the seventh framework programme, grant No. 608466. Data supporting the results reported in this paper may be available on request.

References

ABB, 2016. Micro inverters Available at: https://library.e.abb.com/public/0ac164c3b03678c085257cbd0061a446/MICRO-CDD_BCD.00373_EN.pdf (Accessed: October, 2016).

Balocco, C., 2002. A simple model to study ventilated facades energy performance. Energy Build. 34 (5), 469–475.

Benemann, J., Chehab, O., Schaar-Gabriel, E., 2001. Building-integrated PV modules. Sol. Energy Mater. Sol. Cells 67 (1–4), 345–354.

Crawley, D.B., Hand, J.W., Kummert, M., Griffith, B.T., 2005. Contrasting the capabilities of building energy performance simulation programs. University of Strathclyde, University of Wisconsin, and U.S. Department of Energy.

Crawley, D.B., Hand, J.W., Kummert, M., Griffith, B.T., 2008. Contrasting the capabilities of building energy performance simulation programs. Build. Environ. 43 (4), 661–673.

DECC, 2008. Climate Change Act 2008. Department of Energy and Climate Change, London.

Dolara, A., Leva, S., Manzolini, G., 2015. Comparison of different physical models for PV power output prediction. Sol. Energy 119, 83–99.

EnergyPlus,, 2011. Engineering Reference: The Reference to EnergyPlus Calculations. Lawrence Berkeley National Laboratory, Berkeley.

Fossa, M., Ménézo, C., Leonardi, E., 2008. Experimental natural convection on vertical surfaces for building integrated photovoltaic (BIPV) applications. Exp. Therm. Fluid Sci. 32 (4), 980–990.

Gaillard, L., Giroux-Julien, S., Ménézo, C., Pabiou, H., 2014. Experimental evaluation of a naturally ventilated PV double-skin building envelope in real operating conditions. Sol. Energy 103, 223–241.

Gibbons, J.D., Chakraborti, S., 2014. Nonparametric Statistical Inference, Fourth Edition: Revised and Expanded. fourth ed. Taylor and Francis, Hoboken.

Feustel, H.E., 1999. COMIS—an international multizone air-flow and contaminant transport model. Energy Build. 30 (1), 3–18.

Han, J., Lu, L., Peng, J., Yang, H., 2013. Performance of ventilated double-sided PV façade compared with conventional clear glass façade. Energy Build. 56, 204–209.

Hollander, M., Wolfe, D.A., 1999. Nonparametric Statistical Methods. John Wiley & Sons, New York.

Infield, D., Eicker, U., Fux, V., Mei, L., Schumacher, J., 2006. A simplified approach to thermal performance calculation for building integrated mechanically ventilated PV facades. Build. Environ. 41 (7), 893–901.

Kalogirou, S.A., 2001. Use of TRNSYS for modelling and simulation of a hybrid pv–thermal solar system for Cyprus. Renew. Energy 23 (2), 247–260.

Klein, S.A., Beckman, W.A., Mitchell, J.W., Duffie, J.A., Duffie, N.A., Freeman, T.L., Mitchell, J.C., Braun, J.E., 2009. TRNSYS 17: A Transient System Simulation Program: Mathematical Reference. Solar Energy Laboratory, University of Wisconsin, Wisconsin.

Lau, G.E., Yeoh, G.H., Timchenko, V., Yueen, R.K.K., 2011. Natural Convection in a PV-Integrated Double-Skin Façade using Large-Eddy Simulation. Proc. Eng. 14, 3277–3284.

Lilliefors, H.W., 1969. On the Kolmogorov-Smirnov Test for the Exponential Distribution with Mean Unknown. J. Am. Statist. Assoc. 64 (325), 387–389.

Mei, L., Infield, D., Eicker, U., Fux, V., 2003. Thermal modelling of a building with an integrated ventilated PV façade. Energy Build. 35 (6), 605–617.

Mellit, A., Massi Pavan, A., Lughi, V., 2014. Short-term forecasting of power production in a large-scale photovoltaic plant. Sol. Energy 105, 401–413.

Neymark, J., Judkoff, R., 2004. Building Energy Simulation Test and Diagnostic Method for Heating, Ventilation, Air Conditioning Equipment Models-HVAC BESTEST. National Renewable Energy Laboratory, Golden, Colorado.

Omer, S.A., Wilson, R., Riffat, S.B., 2003. Monitoring results of two examples of building integrated PV (BIPV) systems in the UK. Renew. Energy 28 (9), 1387–1399.

Orme, M., Liddament, MW., Wilson, A., Air, I., Ventilation, C., 1998. International Energy Agency. Energy Conservation in, B., Community Systems, P., 1998. Numerical Data for Air Infiltration and Natural Ventilation Calculations. Air Infiltration and Ventilation Centre, Coventry.

Peng, J., Curcija, D.C., Lu, L., Selkowitz, S.E., Yang, H., Zhang, W., 2016. Numerical investigation of the energy saving potential of a semi-transparent photovoltaic double-skin facade in a cool-summer Mediterranean climate. Appl. Energy 165, 345–356.

REELCOOP, 2015. Research Cooperation in Renewable Energy Technologies for Electricity Generation report. Seventh Framework Programme of the European Union.

Skoplaki, E., Palyvos, J.A., 2009. On the temperature dependence of photovoltaic module electrical performance: a review of efficiency/power correlations. Sol. Energy 83 (5), 614–624.

TESS, 2010. TESSLibs-17: Component Libraries for the TRNSYS Simulation Environment. Thermal Energy Systems Specialists, Wisconsin.

TRNSYS, 2010. TRNSYS 17: A Transient System Simulation Program-Weather Data. University of Wisconsin, Wisconsin, Solar Energy Laboratory.

TRNFLOW, 2009. A Module of an Air Flow Network for Coupled Simulation-Manual. Transsolar Energietechnik, Stuttgart.

UKPV, 2009. 2020 a Vision for UK PV: An up to Date and Accurate Analysis on the Investment Case for Solar Photovoltaics (PV) in the UK. UK Photovoltaic Manufacturers Association, London.